PCCP

PAPER

View Article Online
View Journal | View Issue

Cite this: *Phys. Chem. Chem. Phys.*, 2014, **16**, 4771

Hydrogen bonding in microsolvation: photoelectron imaging and theoretical studies on Au_x^-–$(H_2O)_n$ and Au_x^-–$(CH_3OH)_n$ (x = 1, 2; n = 1, 2) complexes†

Xia Wu,‡[a] Kai Tan,‡[b] Zichao Tang*[a] and Xin Lu*[b]

Received 1st May 2013,
Accepted 9th January 2014

DOI: 10.1039/c3cp51851e

www.rsc.org/pccp

We have combined photoelectron velocity-map imaging (VMI) spectroscopy and theoretical calculations to elucidate the geometry and energy properties of $Au_x^-(Solv)_n$ clusters with x = 1, 2; n = 1, 2; and Solv = H_2O and CH_3OH. Besides the blue-shifted vertical electron detachment energies (VDEs) of the complexes $Au_{1,2}^-(Solv)_n$ with the increase of the solvation number (n), we independently probed two distinct $Au^-(CH_3OH)_2$ isomers, which combined with MP2/aug-cc-pVTZ(pp) calculations represent a competition between O···H–O hydrogen bonds (HBs) and Au···H–O nonconventional hydrogen bonds (NHBs). Complementary calculations provide the total binding energies of the low-energy isomers. Moreover, the relationship between the total binding energies and total VDE_{shift} is discussed. We found that the $Au_{1,2}^-$ anions exhibit halide-analogous behavior in microsolvation. These findings also demonstrate that photoelectron velocity map imaging spectroscopy with the aid of the *ab initio* calculations is an effective tool for investigating weak-interaction complexes.

Introduction

Since the discovery of the high catalytic behavior of gold nanoparticles during oxidation of CO at low temperatures,[1] many unique chemical characteristics of gold clusters and nanoparticles have been found with potential applications, in which the gold nanoparticles were affected by the biological environment and solution phase or condensed phase chemistry.[2] It is noted that solvent configuration can have a profound impact on the reactions of small clusters,[3] and it needs to be paid more attention. These weak interactions are intriguing and evoke many studies showing that size-selected solvated ionic clusters, formed by the ions and a few number of molecules, acted as a useful simplified model to provide molecular level information about interactions between the solvent and solute molecules.[2,4–6] However, the nature of these weak interactions remains obscure. Here we chose water (H_2O) and methanol (CH_3OH) as the typical polar solvent molecules to study the interaction of the $Au_{1,2}^-$ anion with as few as one and two molecules.

These microsolvation studies of $Au_{1,2}^-$ anions are rarely reported. To the best of our knowledge, there are no published reports on microsolvation of $Au_{1,2}^-$ anions with methanol molecules. For water, Zheng *et al.*[7] reported the anion photoelectron spectra of $Au^-(H_2O)_{1,2}$ and $Au^-(D_2O)_{1-4}$. The infrared photodissociation spectroscopy[8] and vibrational Raman spectroscopy[9] of $Au^-(H_2O)$ showed that the gold anion is bound to the water molecule by a single ionic hydrogen bond, similar to the results of the halide–water complexes.[10] The gold anion tends to play the role of a proton acceptor and forms a Au···H–O bond, named a nonconventional hydrogen bond (NHB),[11,12] which has been realized in many systems including transition metals and noble metals, such as Co, Rh, Ni, Cu, Ag and Au.[11,13] However, it is difficult to accurately describe the strength of these NHBs, which need further experimental and theoretical investigation. Additionally, gold has the highest electron affinity (EA) of all metals, approaching the values of the halogens;[14] and it is also a pseudohalogen and forms an entire class of auride (Au(I)) compounds.[8,15] Many parallel properties were also found between aurides Au^- and halides X^- (X = Cl, Br, I) in the bulk phase, for example, compound CsAu was assigned to have a structure of the CsCl type.[16] This suggests a halide-analogous characteristic of the auride anion and evokes the other points of comparison between Au^- and Cl^- ions.

To explore the obscure nature of weak interactions, the conventional hydrogen bond (HB, O···H–O) and the NHB

[a] *State Key Laboratory of Molecular Reaction Dynamics, Dalian Institute of Chemical Physics, Chinese Academy of Sciences, Dalian 116023, China. E-mail: ztang@dicp.ac.cn*

[b] *Collaborative Innovation Center of Chemistry for Energy Materials, State Key Laboratory of Physical Chemistry of Solid Surfaces & Fujian Provincial Key Laboratory of Theoretical and Computational Chemistry, Department of Chemistry, College of Chemistry and Chemical Engineering, Xiamen University, Xiamen 361005, China. E-mail: xinlu@xmu.edu.cn; Fax: +86-592-2183047*

† Electronic supplementary information (ESI) available. See DOI: 10.1039/c3cp51851e

‡ These authors contributed equally to this work.

(Au···H–O), and to confirm the halide-analogous character, we employed anion photoelectron velocity map imaging (VMI)[17] with the aid of *ab initio* calculations. The photoelectron VMI is sensitive to the low kinetic energy electrons with high energy resolution. The high energy resolution guarantees the efficient detection of weak interactions and extends to the study of the cluster complexes. Here we present a joint experimental and theoretical study on the interaction within Au_x^- (x = 1, 2) anion complexes with water and methanol molecules, $Au_{1,2}^-(H_2O)_n$ and $Au_{1,2}^-(CH_3OH)_n$ (n = 1, 2), respectively. *Ab initio* calculations have been carried out to explore structural and energetic aspects of these complexes. On the basis of the photoelectron VMI results with the aid of *ab initio* calculations, the strength of NHB and the analogous behavior between the gold anions and halide anions are discussed.

Experimental and theoretical details

Experimental details

The experiments were performed on our collinear photoelectron VMI spectrometer with a laser vaporization source, which has been described previously in detail.[18] Briefly, the anions were generated by laser vaporization of a pure gold target (99.99%) in the presence of a supersonic beam of helium–water or helium–methanol gas mixture by a pulsed valve. Produced anions were steered to a Wiley–McLaren time-of-flight mass spectrometer (TOFMS),[19] mass selected, and detached by a 355 nm linearly polarized laser beam from a pulsed Nd:YAG laser. The photoelectrons produced by anion–laser interaction were extracted collinearly by a modified velocity map imaging (VMI) repeller electrode, first developed by Eppink and Parker,[17] and recorded (2D image) using the imaging detector. Each image was collected with more than 20 000 laser shots at the 10 Hz repetition rate. The three-dimensional images were reconstructed using the Basis Set Expansion (BASEX) inverse Abel transform method[20] to obtain the photoelectron spectra and angular distributions. The known spectrum of Au^- was used for the spectrometer calibration. The energy resolution was better than 50 meV at an electron kinetic energy (eKE) of 1 eV.

Computational details

The structures and electronic properties of the Au_x^-–$(H_2O)_n$ and Au_x^-–$(CH_3OH)_n$ (x = 1, 2; n = 1, 2) complexes were calculated at the second order Møller–Plesset perturbation theory (MP2) level.[21] Two basis sets were employed: aug-cc-pVTZ(pp) with the small core pseudopotentials for gold[22] and aug-cc-pVTZ for all other atoms.[23] Geometry optimizations without any symmetry constraints and harmonic frequency analyses were performed to verify optimized minima. Each total binding energy (E_b) was calculated as the difference between the energy of the complexes and the sum of the energy of the monomers. To get the best results for binding energies, the basis set superposition error (BSSE) was estimated and corrected using the counterpoise method.[24] Natural bonding orbital (NBO) approach[25] was also performed to calculate the charge distribution. All the above calculations were carried out using the Gaussian03 software package.[26] Additionally, the nature of chemical bonding between the Au^- and Solv (Solv = H_2O, CH_3OH) fragments was obtained by means of the energy partitioning analysis (EPA) method,[27] which was performed at the BP86(ZORA)/QZ4P level of theory in the ADF2007.01 program.[28] The total interaction energy ΔE_{int} corresponds to the energy change when the constituting fragments are combined to form the overall molecule, and can be decomposed into three physically meaningful parts:

$$\Delta E_{int} = \Delta E_{elstat} + \Delta E_{Pauli} + \Delta E_{orb}$$

ΔE_{elstat} is the electrostatic interaction energy between the fragments with unrelaxed electron densities, ΔE_{Pauli} denotes the Pauli repulsion energy between the fragments, and ΔE_{orb} is the orbital interaction energy between the fragments due to the relaxation of Kohn–Sham orbitals in the SCF procedure.

Results and discussion

Photoelectron imaging

The VMI results of $Au^-(Solv)_{1,2}$ and $Au_2^-(Solv)_{1,2}$ (Solv = H_2O, CH_3OH) obtained at 355 nm are shown in Fig. 1 and 2, respectively. Each photoelectron spectrum (PES) is plotted against the electron binding energy (eBE), *i.e.*, the difference between the photon energy (hv) and the electron kinetic energy (eKE). Because of the low photon energy, each spectrum exhibits only the transition from the ground electronic state of the anion to that of the neutral one.

In Fig. 1a and b, the prominent peaks of $Au^-(H_2O)$ and $Au^-(H_2O)_2$ are centered at 2.78 and 3.20 eV, respectively, the corresponding vertical detachment energies (VDEs) obtained from the ground state peak maxima, which agree well with the previous photoelectron spectroscopy values of 2.76 and 3.20 eV, respectively.[7] In comparison with Au^- (see Fig. S1a in the ESI†),

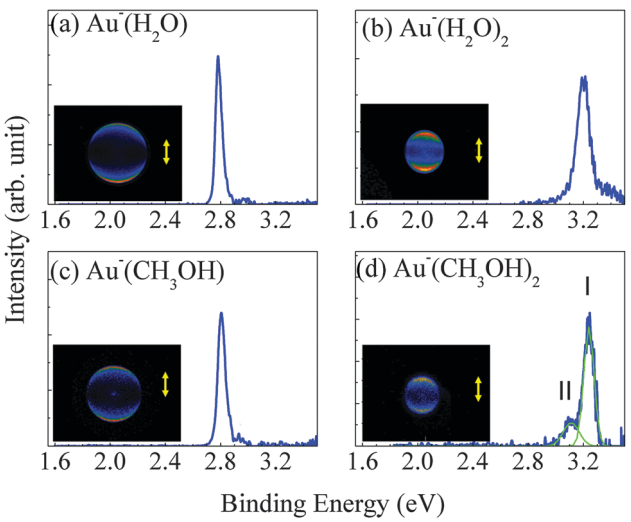

Fig. 1 Photoelectron spectra calculated from the reconstructed images of $Au^-(H_2O)_{1,2}$ and $Au^-(CH_3OH)_{1,2}$. The insets (bottom left) show the raw images. The double arrows show the directions of the laser polarization.

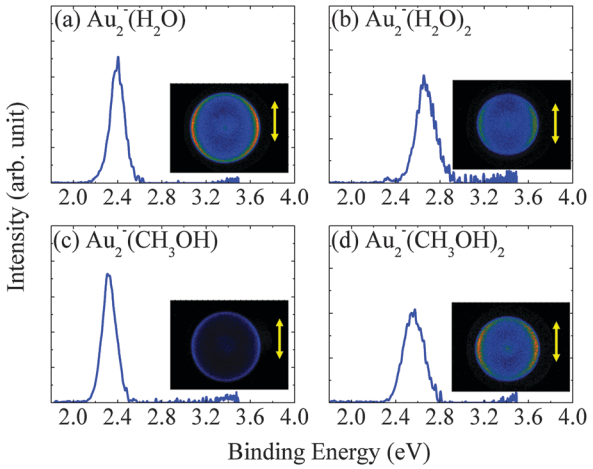

Fig. 2 Photoelectron spectra calculated from the reconstructed images of $Au_2^-(H_2O)_{1,2}$ and $Au_2^-(CH_3OH)_{1,2}$. The insets (bottom right) show the raw images. The double arrows show the directions of the laser polarization.

the VDE blue-shifts 1 and 2 ($VDE_{shift}(1)$ and $VDE_{shift}(2)$) are 0.47 and 0.42 eV for adding the first and second water molecules, while the spectrum fingerprints are similar. Moreover, a weak band (Fig. 1a) of $Au^-(H_2O)$ at 2.974 eV, 194 meV higher binding energy than the main peak (2.78 eV), is observed and is assigned to the H_2O bending vibrational mode, similar to that in the $Cu^-(H_2O)$ case.[29] The PES full width of half-maximum (FWHM) of Au^-, $Au^-(H_2O)$ and $Au^-(H_2O)_2$ are 40, 50, and 90 meV, respectively. The PES not only shifted to higher binding energies but also broadened with the increase in the number of water molecules.

Let us now explore the case of gold–methanol clusters. The VMI of $Au^-(CH_3OH)$ in Fig. 1c is comparable to that in the $Au^-(H_2O)$ cluster, except a little more $VDE_{shift}(1)$ by 0.03 eV. Moreover, a weak peak at 2.96 eV in Fig. 1c is 0.15 eV higher in energy than the prominent peak, assigned to the excitation of methanol during the photodetachment process. For $Au^-(CH_3OH)_2$, it is surprising that the photoelectron spectrum exhibits two peaks (labeled as I, II in Fig. 1d) located at 3.24 and 3.11 eV, and the $VDE_{shift}(2)$ are 0.43 (peak I) and 0.30 eV (peak II), respectively. The FWHM values of peaks I and II of $Au^-(CH_3OH)_2$ are 74 and 116 meV. The large FWHM of peak II indicates significant differences in the geometry of the anion and the neutral species due to the detachment of electrons. All these features of $Au^-(CH_3OH)_2$ in Fig. 1d suggest the coexistence of the low-energy isomers.

Next we examine the evolution of the solute motifs when a second gold atom is added to Au^- to form the Au_2^- diatomic species. Similar to $Au^-(Solv)_n$, the spectra of $Au_2^-(H_2O)_{1,2}$ and $Au_2^-(CH_3OH)_{1,2}$ (Fig. 2) shifted sequentially to higher binding energies and became broadened as the solvent molecular number increased. The VDEs for $Au_2^-(Solv)$ (Solv = H_2O, CH_3OH) are 2.32 and 2.40 eV, with the $VDE_{shift}(1)$ of 0.31 and 0.39 eV, respectively. The VDEs of $Au_2^-(Solv)_2$ are 2.56 and 2.67 eV, with the $VDE_{shift}(2)$ of 0.24 and 0.27 eV, respectively. Compared with the corresponding $VDE_{shift}(n)$ of $Au^-(Solv)_n$, the $VDE_{shift}(n)$s of $Au_2^-(Solv)_n$ are smaller, although the differences between the solvation of a spherical anion Au^- and a rod-like anion Au_2^- are expected. Additionally, in both cases, the FWHMs show a significant increase when a second solvent molecule was added.

Besides the VDE blue-shift and the broadened spectra, the anisotropy parameters (β) are collected in Table 1. The β values of $Au^-(Solv)_{1,2}$ are between 1.7 and 1.1, corresponding to parallel transition, similarly to the ground state transition of Au^- (β = 1.9). The photoelectrons of the $Au_2^-(Solv)_{1,2}$ are ejected perpendicularly to the electric vector of the linear light (E), with the experimental values β = −0.2 to −0.5. The decreases in β with the increase in the number of solvent molecules follow a similar pattern in the cases of water and methanol. This suggests that the nature of the solvent molecule does not significantly alter the angular distribution of the photoelectrons around the solute ion.

Calculated structures and binding energies

Fig. 3 and 4 present the low-energy isomers of the $Au_{1,2}^-(H_2O)_n$ and $Au_{1,2}^-(CH_3OH)_n$ (n = 1, 2) complexes at the MP2/aug-cc-pVTZ (pp) level. In Fig. 3, the optimal geometry of $Au^-(H_2O)$ **1**

Table 1 The experimental[a] and theoretical[b] vertical detachment energies (VDEs), full width of half-maximum (FWHM) in spectra, and the anisotropy parameters (β) at 355 nm for $Au_{1,2}^-(Solv)_n$ (Solv = H_2O, CH_3OH, n = 0–2)

		H_2O				CH_3OH			
		VDE (eV)				VDE (eV)			
	n	Expt	Theor	FWHM (meV)	β	Expt	Theor	FWHM (meV)	β
Au^-	0	2.31(7)	2.26	40	1.9	2.31(7)	2.26	40	1.9
	1	2.78(4)	2.88	50	1.6	2.81(3)	2.93	53	1.7
	2	3.20(1)	3.44	90	1.3	3.24(1)	3.53(**4a**)	74	1.1
						3.11(2)	3.36(**4b**)	116	
Au_2^-	0	2.01(7)	1.86	90	0	2.01(7)	1.86	90	0
	1	2.40(5)	2.27	130	−0.3	2.32(6)	2.18	128	−0.2
	2	2.67(4)	2.71(**6a**)	170	−0.5	2.56(5)	2.51(**8a**)	185	−0.4
			2.59(**6b**)				2.42(**8b**)		

[a] Experimental VDE is measured from the peak maximum of the ground state transition. The error is estimated by considering the instrumental resolution dependent on the electron kinetic energy: eKE × 0.05. [b] MP2/aug-cc-pVTZ(pp) calculations.

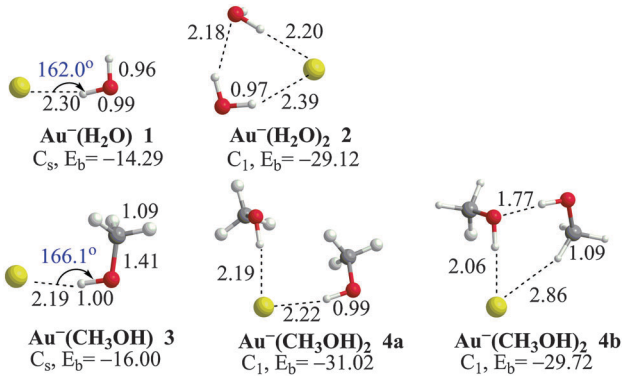

Fig. 3 MP2-predicted geometry (distance in Å, angle in degree) and total binding energy (E_b, kcal mol^{-1}) of $Au^-(H_2O)_n$ and $Au^-(CH_3OH)_n$ (n = 1, 2) complexes.

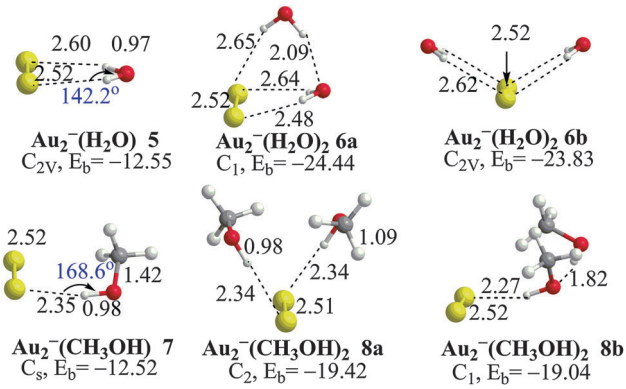

Fig. 4 MP2-predicted geometry (distance in Å, angle in degree) and total binding energy (E_b, kcal mol^{-1}) of $Au_2^-(H_2O)_n$ and $Au_2^-(CH_3OH)_n$ (n = 1, 2) complexes.

adopts a C_s-symmetric structure where the water molecule is cocked with one OH bond toward the gold and the other hydrogen is free, in accordance with the CCSD(T) calculation results.[8] The $Au^-(CH_3OH)$ **3** resembles $Au^-(H_2O)$. In both cases, the Au anion acts as a nonconventional proton acceptor with respect to the conventional O–H donor group and forms one Au···H NHB. Each NHB bond length is significantly shorter than the sum of van der Waals radii of H and Au atoms (~2.68 Å), indicating a strong ion–solvent interaction.

$Au^-(H_2O)_2$ **2** (Fig. 3) has a ground-state structure that the two water molecules with the Au anion form a C_1 6-membered ring, with one water adopting a double-donor (DD) arrangement and the other acting as a acceptor–donor (AD). It forms two Au···H NHBs and one conventional O···H HB. It should be noted that these binding motifs of $Au^-(H_2O)_{1,2}$ are similar to those in the series of halide–water $X^-(H_2O)_{1,2}$ (X = Cl, Br, I) complexes.[9,30]

It is intriguing to discuss the geometry of $Au^-(CH_3OH)_2$, since the photoelectron spectrum indicates the coexistence of the low-energy isomers. Indeed, the calculations show two types of structures: an open structure where both methanol molecules are attached independently to the Au anion and an asymmetric structure where the Au anion is linked to a methanol dimer. Au^- acts as a double acceptor for the open structure (Fig. 3, **4a**), both methanol molecules are in the primary solvation shell, forming two NHBs with bond lengths of 2.19 and 2.22 Å, respectively. The asymmetric structure (Fig. 3, **4b**) forms a NHB (2.06 Å) and a HB (1.77 Å), where Au^- acts as a single acceptor. The NHB bond length in the asymmetric structure is much shorter and stronger than those in the open structure. This strengthening in the asymmetric form arises from the cooperative effect, which was accepted in the asymmetric isomer of $I^-(CH_3OH)_2$.[31] More importantly, these two isomers of $Au^-(CH_3OH)_2$ indicate a competition for the HB *versus* the NHB.

For $Au_2^-(H_2O)$ **5** in Fig. 4, each Au anion acts as a non-conventional proton acceptor, and the H_2O is attached to Au_2^- *via* two equal NHBs (2.60 Å), similar to that of $X_2^-(H_2O)$ (X = Cl, Br, I).[32–34] For $Au_2^-(H_2O)_2$, two nearly isoenergetic conformers considered either as a water dimer or as separated water monomers were obtained after optimization. $Au_2^-(H_2O)_2$ **6a** with the water dimer bridging the Au_2^- is the more stable form. The $Au_2^-(H_2O)_2$ **6b** with two separated water molecules on either side of Au_2^- lies 0.61 kcal mol^{-1} higher in energy than the former. The four equal NHB bond lengths are 2.62 Å. These close isomers cannot be distinguished due to the broad spectrum. Not surprisingly, the binding motifs of $Au_2^-(H_2O)_2$ are also analogous to those in $X_2^-(H_2O)_2$ (X = Cl, Br, I).[32–34]

For $Au_2^-(CH_3OH)$, the only NHB bond length is 2.35 Å. For $Au_2^-(CH_3OH)_2$, the more stable form is isomer **8a** with two separated methanol molecules on either side of Au_2^-, and both the NHB bond lengths are 2.34 Å. Another isomer **8b** is higher in energy, where the methanol dimer connects with the Au_2^-, the NHB bond length is also shortened due to the cooperative effect. Although there are no published reports on $X_2^-(CH_3OH)_{1,2}$ (X = Cl, Br, I), the similarities between $X_2^-(CH_3OH)_{1,2}$ (X = Cl, Br, I) and $Au_2^-(CH_3OH)_{1,2}$ are expected.

On the other hand, the near linear Au···H–O of $Au^-(H_2O)$ (bond angle: 162.0°), $Au^-(CH_3OH)$ (bond angle: 166.1°), and $Au_2^-(CH_3OH)$ (bond angle: 168.6°) also agree with the description of NHBs,[28] except that of $Au_2^-(H_2O)$. On the basis of the optimal geometry, the calculated total binding energies (E_b) with BSSE correction provide the comparison between the strength of the ion–solvent and solvent–solvent interactions. When the first solvent molecule is added, the cluster experiences only ion–solvent interactions and the bond is of the NHB type. The MP2-computed binding energy E_b values may be used as an estimate of the strength of the NHBs. This can be explained by the following analysis: in $Au^-(H_2O)$ **1**, the NHB length is 2.30 Å and the E_b is −14.29 kcal mol^{-1} and in $Au_2^-(H_2O)$ **5**, both NHB lengths are 2.60 Å and the E_b is −12.55 kcal mol^{-1}. This implies that a longer NHB length causes an increase in the energy content of the cluster, making it somewhat loosely bound. The NHB length and the E_b of $Au^-(CH_3OH)$ are 2.19 Å and −16.00 kcal mol^{-1}, respectively. These are more robust than those of $Au_2^-(CH_3OH)$. All these NHB interactions are strong. When two solvent molecules are added to the gold anion, the cluster now experiences solvent–solvent interactions (forming HB) as well as ion–solvent

interactions (forming NHB). Steric effects between the solvent molecules will cause a competition between these two concurrent events. The isoenergetic isomers resulted from the competition between HB and NHB. The binding energy of $Au^-(H_2O)_2$ is much stronger than that (-4.71 kcal mol^{-1}) of the $(H_2O)_2$ dimer, which is calculated at MP2/aug-cc-pVTZ. It indicates that the ion–solvent interaction (NHB) of $Au^-(H_2O)_2$ is dominated, and there are no isomers resulted from competition for $Au^-(H_2O)_2$. For $Au^-(CH_3OH)_2$, the strength of NHB is a little stronger than that of HB. The NHB in $Au_2^-(Solv)_2$ complexes have a nearly same strength as the HB. Thus these comparable competitions between HB and NHB lead to the existence of isoenergetic isomers of $Au^-(CH_3OH)_2$ and $Au_2^-(Solv)_2$.

Besides, the theoretical and experimental VDEs of $Au_{1,2}^-(H_2O)_n$ and $Au_{1,2}^-(CH_3OH)_n$ (n = 1, 2) are collected and compared in Table 1. Within the experimental uncertainty, the trends of calculated VDEs are consistent with those of the measured VDEs. The comparison of experimental and calculated VDE values confirm the reliable results at the MP2/aug-cc-pVTZ(pp) theoretical level. For these anion–molecule complexes, the VDE values are blue-shifted. In other words, the anion is stabilized by the neutral solvent molecules. Here, total VDE_{shift} was defined by the difference between VDE(n) and VDE(0). Thus, both the total VDE_{shift} and values of the total binding energies can represent the solvation energy to a large extent. Fig. 5 shows the calculated total binding energies as a function of the calculated total VDE_{shift} of the title complexes. For comparison, the available values[9,35] of $X^-(H_2O)$ (X = Cl, Br, I) are also displayed. In Fig. 5a, all the values of $X^-(Solv)_{1,2}$ are approximately located at the $y = x$ line, showing a clear linear relationship. The binding energy ($E_b(1)$) is almost equal to total $VDE_{shift}(1)$, while the binding energies ($E_b(2)$) are a little higher than the total VDE_{shift} as a result of the stabilization effect of the solvent–solvent interaction. In other words, the deviation from the linear relationship with total $VDE_{shift}(2)$ is due to a competition for HB *versus* NHB.[6] The total binding energy of $Au^-(H_2O)$ is located between the $Br^-(H_2O)$ and $I^-(H_2O)$. The behavior of the $Au_2^-(Solv)_{1,2}$ in Fig. 5b is similar, except the smaller E_b and total VDE_{shift} values than those of $Au^-(Solv)_{1,2}$. The numerical decrease represents qualitatively weak ion–solvent interaction.

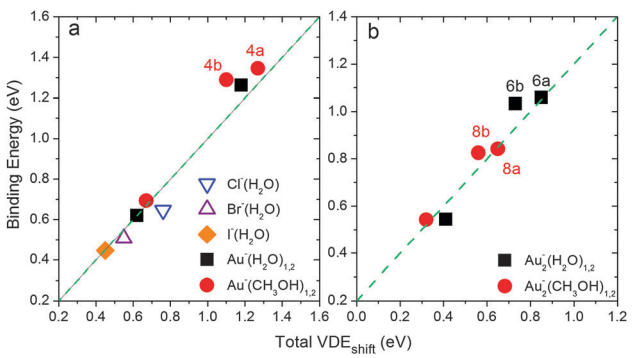

Fig. 5 MP2-predicted values of total binding energies (E_b) *versus* total VDE_{shift} of the title complexes; the E_b and total VDE_{shift} values of $X^-(H_2O)$ (X = Cl, Br, I) are from ref. 9 and 35.

For these typical systems, the total VDE_{shift} values can roughly be used to estimate the binding energies of the microsolvent, which provides a direct measuring method for binding energies.

Comparison with the hydrated halide series

The geometric analyses of $Au_{1,2}^-(H_2O)_{1,2}$ and $Au_{1,2}^-(CH_3OH)_{1,2}$ evoke the similarities in microsolvation between $Au_{1,2}^-$ and $X_{1,2}^-$ (X = Cl, Br, I). The previous infrared photodissociation spectroscopy[8] of $Au^-(H_2O)$ is also reminiscent of those of halide–water complexes. In order to compare with the halide–water complexes, we collect our results and the available information on these halide–water complexes[9,10,35] in Table 2. It is obvious that all $X^-(H_2O)$ (X = Cl, Br, I, Au) form one NHB, characterized by the bond length R(H–X) and the bond angle ∠O–H–X. It is noticeable that the binding energies and the $VDE_{shift}(1)$ are also close. For $X^-(H_2O)_2$ (X = Cl, Br, I, Au), the optimal geometry structures adopt the cyclic (C_1) network illustrated in Fig. 3. In addition, the optimal geometries of $Au_2^-(H_2O)_{1,2}$ are in accordance with those of $X_2^-(H_2O)_{1,2}$ (X = Cl, Br, I). When the solvent molecule is methanol, we expect the similar results.

The natural charges were obtained by using NBO analysis. In both cases, the extra charges mainly locate in the solute Au or Cl atoms (Table S1 in the ESI†), and the charges on the H atoms are positive indicating the protonic character of the H atoms in both complexes. Each can be described as a closed shell and has a spherical symmetry as a proton acceptor with the H atom, indicating a strong electrostatic interaction. Obviously, all interactions between the Au^- anion and H_2O or CH_3OH are dominated by the electrostatic contribution in these electron donor–acceptor complexes, as in the case of solvation of halide ions.

Based on the NBO natural charge results, the EPA bonding analysis was performed using X^- and $Solv^0$ fragments. Table 3 presents the data of EPA analyses. Of the four selected species examined by the EPA bonding analysis, it is evident that the Cl^-–(Solv) interactions are stronger than the Au^-–(Solv) interactions. This is reflected by the shorter bond lengths in the case of the Cl^-–(Solv) systems. Furthermore, the electrostatic interactions ΔE_{elstat} are the most dominating contributions for all the four species. As a consequence, although the Au^-–(Solv) is a NHB species, it exhibits the characteristics of a conventional electrostatic HB complex. When the solute ion contains more atoms, the extra charge will diffuse and weaken the NHB interaction. It is predicted that competition for the HB *versus*

Table 2 Properties of $X^-(H_2O)$ (X = Cl, Br, I, Au)

X =	Cl	Br	I	Au[d]
Value of total binding energy (eV)	0.65[a]	0.51[a]	0.45[a]	0.62
Experimental VDE_{shift} (1) (eV)	0.76[b]	0.55[b]	0.45[b]	0.47
∠O–H–X (°)	168.9[c]	167.5[c]	165.4[c]	162.0
R(H–X) (Å)	2.12[c]	2.29[c]	2.55[c]	2.30

[a] Measured values from ref. 9. [b] ref. 35. [c] At MP2/aug-cc-pVTZ from ref. 10. [d] This work.

Table 3 Energy decomposition (in kcal mol^{-1}) and bond lengths (in angstroms) for the X^-–(Solv) (X = Au, Cl; Solv = H_2O, CH_3OH) species with fragments (X^- + $Solv^0$)

	ΔE_{int}	ΔE_{Pauli}	ΔE_{elstat}	ΔE_{orb}	Bond length
Au^-–(H_2O)	−13.30	16.02	−18.81	−10.51	2.275
Cl^-–(H_2O)	−15.88	15.92	−20.38	−11.41	2.094
Au^-–(CH_3OH)	−13.83	18.95	−19.83	−12.95	2.232
Cl^-–(CH_3OH)	−17.20	18.95	−21.79	−14.36	2.041

the NHB is critical in microsolvation of $Au_{1,2}^-(H_2O)_n$ and $Au_{1,2}^-(CH_3OH)_n$ systems.

Conclusions

We have presented a combined experimental anion photoelectron velocity map imaging and theoretical MP2 calculations on $Au_{1,2}^-(Solv)_n$ clusters, for n = 1, 2 and Solv = H_2O and CH_3OH. The experimental vertical electron detachment energies (VDEs) were obtained and compared with the *ab initio* calculations. The results show that HBs reflect the interaction between solvents and NHBs, formed in the complexes of the anions Au^- and Au_2^- with H_2O and methanol, reflect ion–solvent interactions. The electrostatic interactions dominate the NHBs, thus Au^- with local charge has stronger interactions with a solvent molecule than that of Au_2^-. The cooperative solvation effect was detected in $Au^-(CH_3OH)_2$, like $X^-(CH_3OH)_2$ (X = Cl, Br, I). The optimal geometry and energy properties of $Au_{1,2}^-(H_2O)_n$ and halide–water complexes represent a similar microsolvation behavior. The halide-analogous microsolvation behavior of Au^- provides a new insight to extend the scope of solvation chemistry. Moreover, the total binding energies in title complexes are approximately linear to the total VDE_{shift}. Then the experimental total VDE_{shift} can be used to estimate the binding energies of the microsolvent, which provides a direct method of measurement for binding energies. The results also confirm the existence of the low-energy isomers of $Au^-(CH_3OH)_2$, which presents competitive HB and NHB interactions. The observed isomers show that the photoelectron imaging is an effective tool for studying those weak interaction complexes.

Acknowledgements

This work was sponsored by NSFC (Grant No. 21103186, 21073186 and 21273177), the Ministry of Science and Technology of China (Grant No. 2011CB808504), and the Chinese Academy of Sciences.

Notes and references

1 M. Haruta, S. Tsubota, T. Kobayashi, H. Kageyama, M. Genet and B. Delmon, *J. Catal.*, 1993, **144**, 175–192.
2 A. W. Castleman and P. Jena, *Proc. Natl. Acad. Sci. U. S. A.*, 2006, **103**, 10554–10559.
3 W. H. Robertson, E. G. Diken, E. A. Price, J. W. Shin and M. A. Johnson, *Science*, 2003, **299**, 1367–1372.
4 O. P. Balaj, C. K. Siu, I. Balteanu, M. K. Beyer and V. E. Bondybey, *Chem.–Eur. J.*, 2004, **10**, 4822–4830.
5 C. K. Siu and Z. F. Liu, *Chem.–Eur. J.*, 2002, **8**, 3177–3186.
6 J. H. Hendricks, H. L. de Clercq, C. B. Freidhoff, S. T. Arnold, J. G. Eaton, C. Fancher, S. A. Lyapustina, J. T. Snodgrass and K. H. Bowen, *J. Chem. Phys.*, 2002, **116**, 7926–7938.
7 W. Zheng, X. Li, S. Eustis, A. Grubisic, O. Thomas, H. de Clercq and K. Bowen, *Chem. Phys. Lett.*, 2007, **444**, 232–236.
8 H. Schneider, A. D. Boese and J. M. Weber, *J. Chem. Phys.*, 2005, **123**, 084307.
9 D. Y. Wu, S. Duani, X. M. Liu, Y. C. Xu, Y. X. Jiang, B. Ren, X. Xu, S. H. Lin and Z. Q. Tian, *J. Phys. Chem. A*, 2008, **112**, 1313–1321.
10 S. Horvath, A. B. McCoy, B. M. Elliott, G. H. Weddle, J. R. Roscioli and M. A. Johnson, *J. Phys. Chem. A*, 2010, **114**, 1556–1568.
11 E. S. Kryachko and F. Remacle, *Chem. Phys. Lett.*, 2005, **404**, 142–149.
12 E. S. Kryachko, in *Self-Organization of Molecular Systems: From Molecules and Clusters to Nanotubes and Proteins*, ed. N. Russo, V. Y. Antonchenko and E. S. Kryachko, Springer, Netherlands, 2009, pp. 315–334.
13 I. Alkorta, I. Rozas and J. Elguero, *Chem. Soc. Rev.*, 1998, **27**, 163–170.
14 J. C. Rienstra-Kiracofe, G. S. Tschumper, H. F. Schaefer, S. Nandi and G. B. Ellison, *Chem. Rev.*, 2002, **102**, 231–282.
15 P. Pyykko, *Angew. Chem., Int. Ed.*, 2002, **41**, 3573–3578.
16 M. T. Raisanen, N. Runeberg, M. Klinga, M. Nieger, M. Bolte, P. Pyykko, M. Leskela and T. Repo, *Inorg. Chem.*, 2007, **46**, 9954–9960.
17 A. Eppink and D. H. Parker, *Rev. Sci. Instrum.*, 1997, **68**, 3477–3484.
18 X. Wu, Z. B. Qin, H. Xie, X. H. Wu, R. Cong and Z. C. Tang, *Chin. J. Chem. Phys.*, 2010, **23**, 373–380.
19 W. C. Wiley and I. H. McLaren, *Rev. Sci. Instrum.*, 1955, **26**, 1150–1157.
20 V. Dribinski, A. Ossadtchi, V. A. Mandelshtam and H. Reisler, *Rev. Sci. Instrum.*, 2002, **73**, 2634–2642.
21 C. Moller and M. S. Plesset, *Phys. Rev.*, 1934, **46**, 618.
22 K. A. Peterson and C. Puzzarini, *Theor. Chem. Acc.*, 2005, **114**, 283–296.
23 J. Thom and H. Dunning, *J. Chem. Phys.*, 1989, **90**, 1007–1023.
24 S. F. Boys and F. Bernardi, *Mol. Phys.*, 1970, **19**, 553–566.
25 E. Glendening, A. Reed, J. Carpenter and F. Weinhold, *Computer Program: Gaussian NBO version 3.1*, University of Wisconsin, Madison, 1998.
26 M. J. Frisch, G. W. Trucks, H. B. Schlegel, G. E. Scuseria, M. A. Robb, J. R. Cheeseman, J. A. Montgomery Jr, T. Vreven, K. N. Kudin, J. C. Burant, J. M. Millam, S. S. Iyengar, J. Tomasi, V. Barone, B. Mennucci, M. Cossi, G. Scalmani, N. Rega, G. A. Petersson, H. Nakatsuji, M. Hada, M. Ehara, K. Toyota, R. Fukuda, J. Hasegawa, M. Ishida, T. Nakajima, Y. Honda, O. Kitao, H. Nakai, M. Klene, X. Li, J. E. Knox, H. P. Hratchian, J. B. Cross, C. Adamo, J. Jaramillo, R. Gomperts, R. E. Stratmann,

O. Yazyev, A. J. Austin, R. Cammi, C. Pomelli, J. W. Ochterski, P. Y. Ayala, K. Morokuma, G. A. Voth, P. Salvador, J. J. Dannenberg, V. G. Zakrzewski, S. Dapprich, A. D. Daniels, M. C. Strain, O. Farkas, D. K. Malick, A. D. Rabuck, K. Raghavachari, J. B. Foresman, J. V. Ortiz, Q. Cui, A. G. Baboul, S. Clifford, J. Cioslowski, B. B. Stefanov, G. Liu, A. Liashenko, P. Piskorz, I. Komaromi, R. L. Martin, D. J. Fox, T. Keith, M. A. Al-Laham, C. Y. Peng, A. Nanayakkara, M. Challacombe, P. M. W. Gill, B. Johnson, W. Chen, M. W. Wong, C. Gonzalez and J. A. Pople, Gaussian, Inc., Pittsburgh, PA, 2004.

27 F. M. Bickelhaupt and E. J. Baerends, *Reviews in Computational Chemistry*, 2000, pp. 1–86.

28 *ADF2007.01, SCM, Theoretical Chemistry*, Vrije Universiteit, Amsterdam, The Netherlands, 2007.

29 G. J. Rathbone, T. Sanford, D. Andrews and W. C. Lineberger, *Chem. Phys. Lett.*, 2005, **401**, 570–574.

30 P. Ayotte, S. B. Nielsen, G. H. Weddle, M. A. Johnson and S. S. Xantheas, *J. Phys. Chem. A*, 1999, **103**, 10665–10669.

31 W. H. Robertson, K. Karapetian, P. Ayotte, K. D. Jordan and M. A. Johnson, *J. Chem. Phys.*, 2002, **116**, 4853–4857.

32 A. K. Pathak, T. Mukherjee and D. K. Maity, *J. Chem. Phys.*, 2007, **127**, 044304.

33 A. K. Pathak, T. Mukherjee and D. K. Maity, *J. Chem. Phys.*, 2007, **126**, 034301.

34 A. K. Pathak, T. Mukherjee and D. K. Maity, *J. Phys. Chem. A*, 2008, **112**, 744–751.

35 G. Markovich, S. Pollack, R. Giniger, O. Cheshnovsky and U. Kaldor, *J. Chem. Phys.*, 1994, **101**, 9344–9353.